The 7th Annual IEEE International Conference on
Cyber Technology in Automation, Control and Intelligent Systems
July 31-August 4, 2017, Hawaii, USA

System Identification and Control of PPUAV

Bingbing Li[1, 2], Liying Yang[1], Yuqing He[1*], Jianda Han[1], Jizhong Xiao[3*]
1 State Key Laboratory of Robotics, Shenyang Institute of Automation, Chinese Academy of Sciences, Shenyang 110016, China
2 University of Chinese Academy of Sciences, Beijing 100049, China
3 The City College, City University of New York, New York, USA

***Abstract*—Powered Parafoil Unmanned Aerial Vehicle(PPUAV), which is suitable for large-area and long-time surveillance and airdrop missions, is a type of innovative UAV. It consists of parafoil canopy, payload and suspension lines, and has the advantages of simple structure, low cost and high load capacity. However, PPUAV has the problems of apparent mass and flexible connection, which makes it hard to build an accurate model for controller design in practical applications. This paper develops an applicable method of modeling to capture the main characteristics of PPUAV, and the proposed model is validated by actual flight test. An adapted PID controller and a guidance algorithm are also proposed based on the model. The simulations show the effectiveness of the control method for applications of PPUAV.**

Keywords—powered parafoil; UAV; model simplification; system identification; feed-forward control; guidance

I. INTRODUCTION

A. Introduction of PPUAV

Powered Parafoil Unmanned Aerial Vehicle (PPUAV) is a small aircraft, which is able to cover large horizontal distances from the release point. It provides a unique capability for air-transport of heave payloads according to the high payload-weight-ratio. PPUAV is compact before parafoil deployment, lightweight, flies at low speed and impacts the ground with low velocity. PPUAV is often considered to be safer than normal fixed-wing aircraft because of its inherent stability, limited response to control inputs, and stall resistance. All of the above advantages make it a suitable platform for field investigations, search and rescue, and delivery[1].

However, the system has the characteristics of complexity, uncertainty, nonlinearity, time variation, large delay and large inertia, and is easily affected by the atmospheric environment[2]. The parafoil is strongly influenced by apparent mass because of its light structure. And a unique feature of PPUAV is the high degree of variability of basic flight dynamic, which causes challenges to practical applications[3].

This work is supported by National Nature Sciences Foundation of China(Grant No. 61503369 and 61528303) / The state key laboratory of robotics / Chinese National Key Technology R&D Program(Grant No. Y4A1208101).

B. Control mechanism

The predominant control mechanism for PPUAV is left and right brake deflection and thrust provided by the engine. The PPUAV turns through the asymmetric deflection of left or right brake. The engine provides thrust to take off and accelerate. Predictable changes in aerodynamic loads is caused by thrust and canopy changes, which is the method of controlling the system. The structure of the vehicle is shown in Fig. 1.

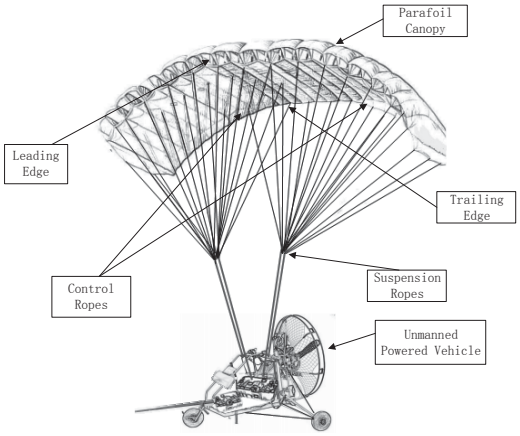

Fig. 1. Structure of PPUAV

For most parafoils, deployment of the right brake causes a significant drag rise and a small lift increase on the right side of the canopy with slight right tilt. The overall effect causes the parafoil to turn right when a right brake is deployed. With a engine installed on the back of the payload, the system can adjust its longitudinal and vertical velocity[4]. To improve the accuracy of the parafoil system, several new flight control mechanisms have been created by

978-1-5386-0490-8/17/$31.00 © 2017 IEEE

dynamic incidence angle control[4,5] and opening vent holes on the upper surface of the canopy to create a virtual aerodynamic spoiler. Symmetric activation of canopy spoilers yields longitudinal control while asymmetric activation creates lateral control. Through the combination of lateral and longitudinal control of the system, the flight control laws are allowed to correct descent rate directly and diminish the final delivery error in landing[6]. In our tests, the control mechanism for the PPUAV is the left and right deflection and the thrust provided by the engine.

C. Researches of PPUAV

Over the past few decades, a lot of models of different parafoil system were developed to address the varied issues. The 3 DOF model[7] is capable to represent some of the most important vehicle characteristics and can be used to principally check the GNC functionality. However, many aspects are not modeled. In turns, the roll angle of the vehicle changes significantly, but is ignored in the model. Horizontal and vertical speed, along with Lift/Drag change with symmetric edge deflection, is considered a constant. The presented 4 DOF model[8] is able to simulate the increasing sink rate during turns and reproduces also the steady effects of symmetric edge deflection on the velocities and Lift/Drag. The 6DOF model describes three inertial position and three Euler orientation angle and the system is considered a rigid body. The 7DOF model is an extension of the 6 DOF model, taking the roll movement with respect to the parafoil into account[9].

And higher models are also developed to measure a more detailed movement, including 8-DOF model[10], 9-DOF model[11], 10-DOF model[12] and 12-DOF model[13].

On another side, a variety of methods have been developed for air vehicle system identification. The two methods that are best suited to the current problem are the output error method (OEM), which is the most common method for parameter identification from noisy measurements, and identification through an extended Kalman filter, which is commonly used when there is both measurement and process noise. These two methods can also be combined to form the filter error method. All of these works approach the problem in slightly different ways, but a common thread among them is the necessity of using a highly instrumented platform specialized for the system identification task in order to obtain sufficient data for successful aerodynamic parameter identification[14].

The paper presents a 6-DOF model and a simplified model (including a longitudinal and a lateral model). The simplified model is then validated using actual flight data. Furthermore, an adapted PID controller and a guidance algorithm are presented for the purpose of executing flight mission. And the algorithms have been run in simulation to prove its effectiveness. Section 2 presents the 6-DOF and a simplified model of PPUAV. Section 3 provides a description of guidance, navigation and control (GN&C), including an adapted PID controller and a guidance algorithm. Then the flight test and simulation results are present in Section 4. The paper ends with conclusions and recommendations for the future development.

II. Mathematical Model of PPUAV

A. Coordinate systems

With the exception of movable parafoil brakes, the parafoil is treated as a rigid body. And the coordinate systems are established. All the coordinate systems are right-hand systems. The inertial coordinate system Σ_G is defined as (X_g , Y_g , Z_g), and the X_g Y_g -plane is horizontal, and the positive direction of Z_g is taken downward as shown in Fig. 2 . The location of the origin and the positive direction of the X_g -axis are appropriately chosen. The canopy coordinate system Σ_C = (X_c , Y_c , Z_c) and payload coordinate system Σ_P = (X_p , Y_p , Z_p) are shown in Fig. 2. The origin C of the coordinate system Σ_C is chosen at the center of gravity (CG) of the canopy. The Z_c -axis is chosen in the direction from C to P (the CG of the payload) and the X_c -axis is taken forward. The origin P of the coordinate system Σ_P is chosen at the CG of the payload. And X_p is taken forward along the direction of the thrust and Z_p is taken downward. In the 6-DOF model, the system is considered as rigid body and the body coordinate system is chosen as Σ_B = (X_b , Y_b , Z_b). The X_b -axis points through the nose of the system and the Z_b -axis is chosen downward in the plane of symmetry of the system with X_b [15].

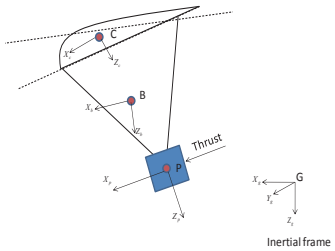

Fig. 2. Coordinate systems

B. 6-DOF model

The 6-DOF model is adopted from [15] and is described in the body frame as follow:

$$m^B \frac{d[v_B^G]^B}{dt} + m^B[\Omega^{BG}]^B[v_B^G]^B = [f]^B \quad (1)$$

and

$$[I_B^B]^B \frac{d[\omega^{BG}]^B}{dt} + [\Omega^{BG}]^B[I_B^B]^B[\omega^{BG}]^B = [M_B]^B \quad (2)$$

where m^B is the mass of the system. $[v_B^G]^B$ is the inertial velocity of the mass center expressed in the body frame. $[\omega^{BG}]^B$ is the rotation velocity of the body frame with respect to the inertial frame expressed in the body frame, and $[\Omega^{BG}]^B$ is the skew-symmetric form of the angular velocity. $[I_B^B]^B$ is the moment of inertia. $[f]^B$, $[M_B]^B$ is the sum of forces and moments about the mass center expressed in the body frame respectively.

C. Model Simplification

A method of model simplification is given in [16]. But the derived model is too simple to describe the characteristics of the system. For the actual maneuver executed, it is able to control the forward velocity, which is not mentioned in that paper. In this paper, the model is simplified as two parts, including a longitudinal model and a lateral model. The lateral model is similar to the one described in [16], but the longitudinal model is changed, which describes not only vertical velocity but also forward velocity. All the models are expressed using transfer functions. In the lateral model, ω denotes yaw angle, S denotes input of asymmetric brake deflection, and g(s) denotes the transfer function from S to ψ. In the longitudinal model, V_{gz} denotes the vertical velocity in inertial frame, and V_{bx} denotes the forward velocity in body frame, T and Sa denote inputs of thrust and symmetric brake deflection, and g_{11}, g_{12}, g_{21}, g_{22} denote the corresponding transfer functions.

The simplified model is described as follow:

Longitudinal model:

$$\omega(s) = g(s) * S(s) \quad (3)$$

Lateral model:

$$\begin{bmatrix} Vgz(s) \\ Vbx(s) \end{bmatrix} \begin{bmatrix} g_{11}(s) & g_{12}(s) \\ g_{21}(s) & g_{22}(s) \end{bmatrix} \begin{bmatrix} T(s) \\ Sa(s) \end{bmatrix} \quad (4)$$

III. CONTROL

The structure of the controller consists of a inner loop PID module and a guidance module. The PID module is used to ensure that the PPUAV will fly the reference trajectory. And the guidance module is used to make trajectory adjustments in response to performance and flight conditions.

A. An adapted PID controller

A PID controller is used to maintain the vertical velocity, forward velocity and yaw rate of the system.

As shown in the model, the inputs have a coupling effect on outputs, which means the variation of a single input will lead to variations of multiple outputs.

Increasing or decreasing the thrust T provided by the engine power affects the longitudinal and vertical velocity. If the trailing edge of the wing is pulled on both sides at the same time, the longitudinal velocity of the aircraft will decrease and the vertical velocity will increase. Deflecting the right or left trailing edge of the parafoil turns the aircraft right or left.

The regulation process using normal PID controller is described here: When the expected vertical velocity increases, the thrust T will increase to decrease the difference between the real value and the expected one, which will also increase the value of forward velocity and will lead to the adjustment of symmetric brake which will also cause change of vertical velocity.

To reduce the coupling effects, a feed-forward controller is designed. In feed-forward control, the input is adjusted to reduce the effect of the disturbances (caused by another input) before they have time to affect the system. The feed-forward controller consists of a time-delay module, a second-order system and a first-order system to ensure execution. And the controller is used to restrain the effect of the variation of the disturbance on the output. The second-order model describes the effect of the disturbance (e.g. T) on the output (e.g. V_{bx}) . The time delay and the time constant of the first-order system are chosen appropriately. Combined the feed-forward controller, it is able to reduce the coupling effects, which makes the previous PID controller more effective. The controller structure is shown in Fig. 3.

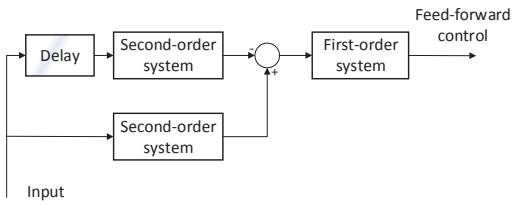

Fig. 3. PID controller structure

B. Guidance

The guidance algorithm splits the flight into 2 main phases: turning and straight flight. The algorithm to straight flight is similar to [16], and the algorithm to turn is to control the yaw rate. While turning, the reference trajectory is given by expected yaw rate. And while straight flight, the reference trajectory is given by expected yaw angle. The logic is shown in Fig. 4, and the algorithm is described as follow:

Turning: Point P denotes the current position, point *v* denotes the current velocity and h denotes vertical distance between current position and expected trajectory, and the expected yaw rate is

$$\omega^* = \frac{v*\sin(\psi-\psi^*)*(\psi-\psi^*)}{h} \tag{5}$$

where ψ denotes the actual yaw angle, and ψ^* denotes the expected yaw angle.

Straight flight: Point P denotes the current position, point T (Tx, Ty) denotes the perpendicular foot, Line MA (A is (Ax, Ay) , M is (Mx, My))denotes the expected trajectory, d denotes the look-ahead distance, and point C (Cx, Cy) denotes the expected position. The guidance algorithm gives an expected yaw angle ψ^*, and the angle is calculated as:

$$Tx = \frac{\frac{(\mathrm{Ax}-\mathrm{Mx})^2*\mathrm{Px}}{\mathrm{Ay}-\mathrm{My}} + (\mathrm{Ax}-\mathrm{Mx})*(\mathrm{Py}-\mathrm{My}) + (\mathrm{Ay}-\mathrm{My})*\mathrm{Mx}}{\frac{(\mathrm{Ax}-\mathrm{Mx})^2}{\mathrm{Ay}-\mathrm{My}} + \mathrm{Ax}-\mathrm{My}} \tag{6}$$

$$Ty = -\frac{(\mathrm{Ay}-\mathrm{My})*\mathrm{Mx} - (\mathrm{Ax}-\mathrm{Mx})*\mathrm{My} - (\mathrm{Ay}-\mathrm{My})*\mathrm{Tx}}{\mathrm{Ax}-\mathrm{Mx}} \tag{7}$$

$$Cx = Tx + d*cos\left(atan2(Ay-My, Ax-Mx)\right) \tag{8}$$

$$Cy = Ty + d*sin\left(atan2(Ay-My, Ax-Mx)\right) \tag{9}$$

$$\psi^* = atan2(Cy-Py, Cx-Px) \tag{10}$$

IV. Flight Test and Simulation

A. Platform structure

PPUAV consists of parafoil canopy, payload, suspension lines and GN&C system. The GN&C system consists of winches, global position system(GPS), magnetic compass, inertial measurement unit(IMU), pitot tube, flight computer and data-transmit module to uplink commands and downlink data. The parameters of the platform are shown in Table 1.

Table 1. System Parameters

Object	Parameter	Value	Units
Canopy	Span	5.92	meters
	Chord	1.66	meters
	Arch	1.14	meters
	Thickness	0.22	meters
	Area	9.8	Sq.mts
	Mass	2.4	kg
Payload	Mass	20	kg

B. System identification

The input-output data is obtained by executing maneuvers in actual flight test: Manual flight test requires a windless environment. The PPUAV was flown to the altitude of 200 m, then the maneuvers were executed after it flied stably. The maneuvers are presented by the percentage of the maximum value of left and right deflection and thrust, and held for a pre-determined time to ensure that the dynamics induced as the result of the maneuver have been damped out: 10/0% (20/0%, 30/0%, 40/0%, 50/0%) flaps for 5 seconds (10 seconds), 0/10% (0/20%, 0/30%, 0/40%, 0/50%) flaps for 5 seconds (10 seconds), 10/10% (20/20%, 30/30%, 40/40%, 50/50%) flaps for 5 seconds(10 seconds), 10%(30%, 50%) thrust for 10 seconds(15 seconds).

The transfer functions obtained are presented as follow:

$$g(s) = \frac{0.0001213s + 0.0002496}{s^2 + 0.9468s + 0.9751} \tag{11}$$

$$g_{11}(s) = \frac{-0.0003046s - 0.001045}{s^2 + 0.2243s + 0.8359} \tag{12}$$

$$g_{12}(s) = \frac{-0.002016s - 0.0002064}{s^2 + 0.8429s + 0.8064} \tag{13}$$

$$g_{21}(s)=\frac{0.0002851s+0.0002664}{s^2+2.159s+0.533} \tag{14}$$

$$g_{22}(s)=\frac{-0.0002958s-0.002586}{s^2+0.775s+1.357} \tag{15}$$

The model is validated by actual flight data as shown in Fig. 4-8. The curves of inputs and outputs have all been transferred to begin at zero. Fig. 4 shows the curve of inputs of symmetric brake deflection and the comparison of actual response curve of forward velocity and simulative response curve. The result is that the mean of the error between actual curve and simulative curve is 0.09, and the variance is 0.019. Fig. 5 shows the curve of inputs of symmetric brake deflection and the comparison of actual response curve of vertical velocity and simulative response curve. The mean of the error between actual curve and simulative curve is -0.001, and the variance is 0.044. Fig. 6 shows the curve of inputs of asymmetric brake deflection and the comparison of actual response curve of yaw rate and simulative response curve. The mean of the error between actual curve and simulative curve is 0.007, and the variance is 0.001. Fig. 7 shows the curve of input of thrust and the comparison of actual response curve of forward velocity and simulative response curve. The mean of the error between actual curve and simulative curve is 0.056, and the variance is 0.015. Fig. 8 shows the curve of input of thrust and the comparison of actual response curve of vertical velocity and simulative response curve. The mean of the error between actual curve and simulative curve is -0.019, and the variance is 0.016. The model fits the flight well proving the validity of the model.

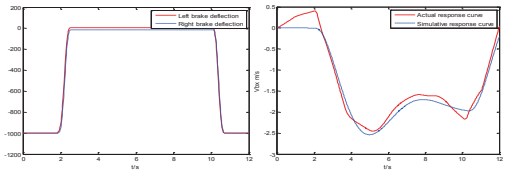

(a) (b)

Fig. 4. (a) Input of symmetric brake deflection; (b) Validation of the model

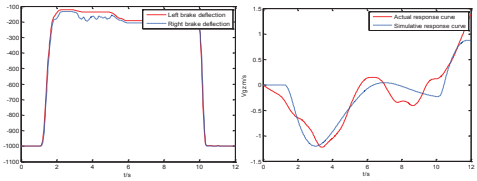

(a) (b)

Fig. 5. (a) Input of symmetric brake deflection; (b) Validation of the model

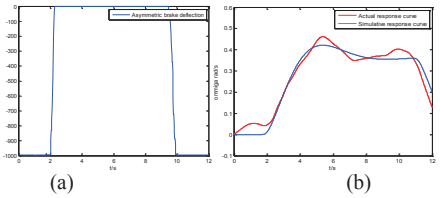

(a) (b)

Fig. 6. (a) Input of asymmetric brake deflection; (b) Validation of the model

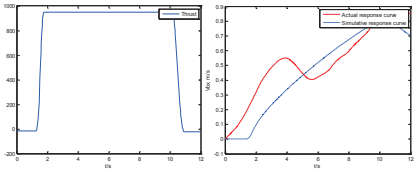

(a) (b)

Fig. 7. (a) Input of thrust; (b) Validation of the model

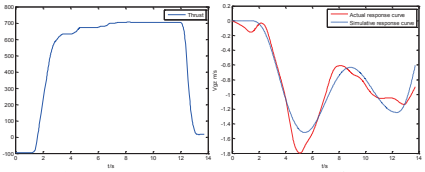

(a) (b)

Fig. 8. (a) Input of thrust; (b) Validation of the model

C. *Control and navigation*

Fig. 9 shows the different results of the same maneuver with and without feed-forward design. The maximum overshoot of the vertical velocity has decreased by 36.8 percent and the results prove the effectiveness of the method.

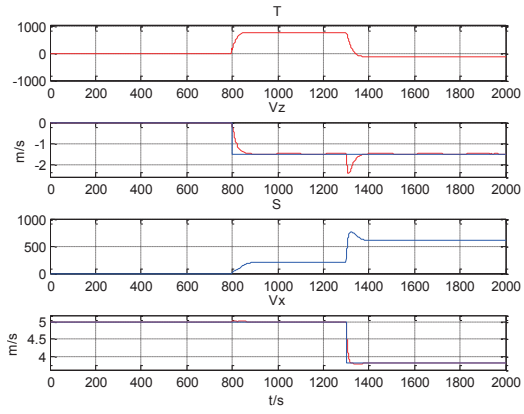

(a)

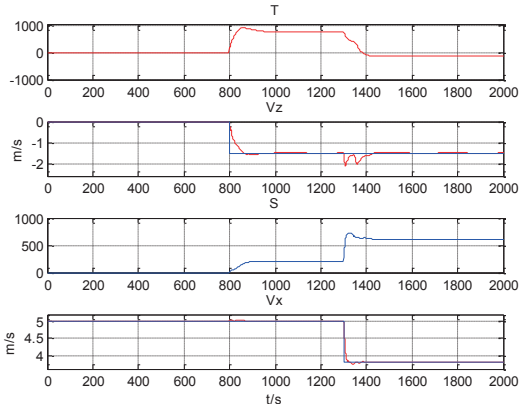

(b)

Fig. 9. (a) Results with feed-forward controller; (b) Results without feed-forward controller

In the test, the expected trajectory is given by 6 expected positions (M, A, B, C, D, E) , and the initial position is [200, 200]. The result is shown in Fig. 10 and validate the effectiveness of the method. But the wind disturbance is not considered and it will be a future work for actual application.

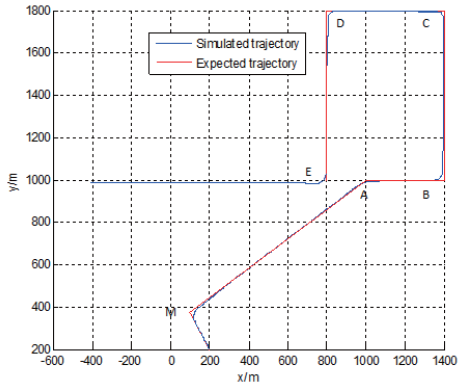

Fig. 10. Flight test in simulation

V. Conclusion and Future Work

This paper has presented a practical method of modeling, system identification, controller design and guidance of PPUAV. A 6DOF model is used as a basic model. A longitudinal and a lateral model are put forward after simplifying. And the models are obtained by system identification using Matlab System Identification Toolbox and validated by actual flight data. Finally, an adapted PID controller and a guidance algorithm are presented to satisfy demand for delivery and surveillance mission, which is validated by simulation.

As the system model in reality is varying and not always the same as the nominal one, an important future work to do is to measure the difference between actual and nominal model, which will need some techniques like state estimation and controller design, which takes model error into account.

References

[1] Devalla, Vindhya, and O. Prakash. Developments in unmanned powered parachute aerial vehicle: A review. Aerospace and Electronic Systems Magazine, IEEE 29.11 (2014): 6-20.

[2] X. Zhi-gang, C. Zi-li,LIU, Yu-tian. Journal of Ordnance Engineering College, 2011, 02: 52-56.

[3] W. Michael, C. Mark, S. Nathan. On the Benefits of In-Flight System Identification for Autonomous Airdrop Systems. Journal of Guidance, Control, and Dynamics.2010, 33(5):1313-1326.

[4] O. A. Yakimenko, Nathan J. Slegers, Robyn A. Tiaden. Development and Testing of the Miniature Aerial Delivery System Snowflake. AIAA Paper 2009-2980, 2009.

[5] N. Slegers, Eric Beyer, Mark Costello. Use of Variable Incidence Angle for Glide Slope Control of Autonomous Parafoils. Journal of Guidance Control and Dynamics, 2008, 31(3): 585-596.

[6] A. Gavrilovski, Michael Ward, Mark Costello. Parafoil Control Authority with Upper-Surface Canopy Spoilers. Journal of Aircraft, 2012, 49(5): 1391-1397.

[7] T, Jann. Aerodynamic model identification and GNC design for the parafoil-load system ALEX. AIAA paper, 2015, 21-24.

[8] W. Gockel, T. Jann. ALEX-Flugdatenauswertung. Entwicklung eines validierten flugmechanischen Modells, DLR Institut fur Flugmechanik, Braunschweig, IB 111-98/47.

[9] C. Gorman, N. Slegers. Comparison and analysis of multi-body parafoil models with varying degrees of freedom. In 21st AIAA Aerodynamic Decelerator Systems Technology Conference and Seminar (pp. 23-26).

[10] N. Slegers, M. Costello. Aspects of control for a parafoil and payload system. Journal of Guidance, Control, and Dynamics, 26(6), 898-905.

[11] M. Hailiang, Q. Zizeng. 9-DoF Simulation of Controllable Parafoil System for Gliding and Stability,". Journal of National University of Defense Technology, 16(2), 49-54.

[12] D. Pillasch, W.Shen, Y.C., Valero, N., "Parachute/Submunition System Coupled Dynamics," AIAA Paper 1984-0784, 8th AIAA ADBT Conference, Hyannis, MA, April 2-4, 1984.

[13] A. Vishnyak. Simulation of the payload-parachute-wing system flight dynamics. AIAA Paper, 1250, 10-13.

[14] M. Ward, M. Costello, N. Slegers. Specialized system identification for parafoil and payload systems. Journal of Guidance, Control, and Dynamics, 35(2), 588-597.

[15] P. Zipfel, Modelling and Simulation of Aerospace Vehicle Dynamics, 2 ed. 1801 Alexander Bell Drive, Reston, VA: American Institute of Aeronautics and Astronautics, 2007.

[16] J. Umenberger, A H. Goktogan. System identification and control of a small-scale paramotor[C]. Robotics and Automation (ICRA), 2013 IEEE International Conference on. IEEE, 2013:2970-2976.